Journal of Applied Research and Technology

www.jart.icat.unam.mx

Journal of Applied Research and Technology 22 (2024) 410-418

Original

Electrochemical performance of YSZ coupled $Ba_{0.5}Sr_{0.5}Fe_{0.9}Cu_{0.1}O_{3-\delta}$ electrode at intermediate temperature

S. Setiyono[a] • F. Fitriana[b] • M. A. Baqiya[a] • S. Suasmoro[a]*

[a]*Department of Physics, Institut Teknologi Sepuluh Nopember, Surabaya, Indonesia*
[b]*Physics Study Program, Universitas Negeri Surabaya, Indonesia*

Received 09 28 2023; accepted 05 14 2024
Available 06 30 2024

Abstract: Synthesis of electrolyte 8% Y_2O_3 stabilized zirconia (YSZ) and characterization of electrical conductivity with BSFC $Ba_{0.5}Sr_{0.5}Fe_{0.9}Cu_{0.1}O_{3-\delta}$ (BSFC) electrode have been conducted. YSZ and BSFC were synthesized using sol-gel self-combustion. YSZ powder was calcined at 700℃ for 2 hours, then pressed into a disk and sintered at 1550 ^{0}C for 6 hours. While BSFC powder was calcined at 850 ℃ for 6 hours and sintered at 1100 ^{0}C for 6 hours. X-ray diffraction (XRD) analysis shows that calcined powder of both YSZ and BSFC has cubic structure possessing space group (Fm-3m) and (Pm-3m), respectively. The lattice parameter of the YSZ a = 5.1677 Å, while the BSFC a = 3.9469 Å. A scanning electron microscope (SEM) shows that BSFC can adhere well to the surface of YSZ. The electrical behavior of the YSZ and half-cell BSFC||YSZ||BSFC exhibit two semi-circles below 200 ℃, three between 250 ℃ and 500 ℃, and two at 550 ℃ and above. These semi-circles are related to the resistance of the grains, the grains boundary of YSZ or YSZ+BSFC, and the electrode. The resistivity decreased with increasing temperature, in which the resistivity of BSFC||YSZ||BSFC is lower than YSZ due to the influence of BSFC. Cathode material BSFC is suitable for YSZ electrolytes.

Keywords: Cole-Cole plot, Debye relaxation, electrolyte YSZ, electrode, impedance

*Corresponding author.
E-mail address: suasm@its.ac.id (S. Suasmoro).
Peer Review under the responsibility of Universidad Nacional Autónoma de México.

1. Introduction

Yttria stabilized zirconia (YSZ) is known as a material fast ionic oxide conductor and is often used as an electrolyte of solid oxide fuel cells (SOFC) and oxygen sensors (Zakaria et al., 2020). This fast ionic conductivity is due to the motion of oxygen vacancies produced by Y^{3+} doped in ZrO_2. Moreover, YSZ has good stability in reductant and oxidant atmospheres, and the 8 mol% yttria doped is known to have a highly stable composition and high conduction in ionic conductivity (Dong & Chen, 2018; Budiana et al., 2016; Peláez-Tirado et al., 2024). The synthesis of YSZ through the solid-state method requires calcination above 1000 ^{0}C until a cubic phase is formed (Budiana et al., 2016). This elevated temperature causes grain growth, and the size of the crystal powder is then large, which is detrimental to further processing. The smaller crystal size will ensure better homogeneity and further processing, hence improving the properties. To attain nanocrystalline size powder, the alternative synthesis route then be exploited, such as sol-gel (Budiana et al., 2016) and microwave hydrothermal (Peláez-Tirado et al., 2024). Another technique includes sol-gel preparation followed by self-combustion (Zarkov et al., 2015) process to synthesize nanoscale has been reported for $PbZrTiO_3$ (Sato et al., 2015). Inspiring this method, by dissolving Y_2O_3 in nitric acid then mixed with $ZrO(NO_3)_2$ and put in the citric acid then brought to self-ignition to get the precursor.

Intermediate temperature solid oxide fuel cell (IT-SOFC) consists of anodes, electrolytes, and cathodes operated at moderate temperatures of 500-600℃. It was reported that $Ba_{0.5}Sr_{0.5}FeO_3$ (BSF) based materials were used for electrodes (Wang et al., 2008; Schäfer et al., 1997), due to their capability in the oxidation-reduction process. In the previous report (Wang et al., 2015a; Wang et al., 2015b), the Cu-doped BSF has excellent conductivity at an intermediate temperature (≈500℃), which is suitable for ITSOFC electrodes. However, it is necessary to examine the adherence of the electrode and electrolyte when it is brought to a cell.

This paper reports the synthesis of electrolyte 0.8 mole % Y doped ZrO_2 and the $Ba_{0.5}Sr_{0.5}Fe_{0.9}Cu_{0.1}O_{3-\delta}$ for an electrode. Then, a half-cell BSFC||YSZ||BSFC was built to examine the suitable BSFC composition as an electrode. The characterization variables include impedance complex analysis in the frequency range 0.1 Hz – 32 MHz at 150 ℃ up to 850 ℃.

2. Materials and methods

The solid electrolyte 8YSZ and electrode BSFC were synthesized using the self-combustion method as described elsewhere (Fitriana et al., 2018; Fitriana et al., 2021). First, the stoichiometric mixture of $ZrCl_4$, Y_2O_3, HNO_3, and $C_6H_8O_7$ as a combustion igniter for electrolyte material. $ZrCl_4$ powder was dissolved in H_2O, and then NH_4OH was poured at once in $Zr(OH)_2$ solution to produce $ZrO_2.nH_2O$ precipitate. The precipitate was then washed up until Cl^- free and dissolved into HNO_3 to make $ZrO(NO_3)_2$ solution. Further, Y_2O_3 was dissolved into HNO_3 to prepare the doped material. These two solutions were then mixed and added by a solution of $C_6H_8O_7{\cdot}2H_2O$ (0.37 gr/cc), then heated at 80 °C while stirred in a magnetic stirrer, increasing gradually until 220 °C for self-combustion. The precursor of YSZ powder was then calcined at 700 ^{0}C for 2 h. Secondly, the powder preparation for the electrode includes a mixture of stoichiometric amounts of $Ba(NO_3)_2$, $Sr(NO_3)_2$, and $Fe(NO_3)_3{\cdot}9H_2O$ dissolved in deionized water at 30°C, while CuO was dissolved in nitric acid. All the saturated solutions were mixed using a magnetic stirrer, and then a citric acid solution was added while stirring to form an aqueous solution. The mixed solution was heated to 100 °C and then increased gradually to 150, 200, and 220 °C before self-combustion occurred to obtain dark precursors. The BSFC precursors were ground and then calcinated at 850 °C for 6 h to get the composition in a well-defined phase and structure.

X-ray diffraction (PHILIP X'pert PMD) was used to identify phases and the structure of both powder and sintered pellets. Data was collected using the Bragg-Brentano principle 0.02^0 step scan, and Cu Kα radiation (λ = 1.541874 Å) operated at 30 mA – 40 kV. The phases of the samples were identified using Match! software, while the structure of samples was analyzed using Rietveld's refinement by Rietica software (Hunter, 2000). On the other hand, the scanning electron microscope (SEM) HITACHI FLEX SEM 100 was utilized to observe the samples' microstructures.

A half-symmetrical cell (cathode||YSZ||cathode) was fabricated to perform an impedance test. The 8YSZ electrolyte calcined powder was pressed in a 13 mm uniaxial die at 40 MPa and sintered at 1550 °C for 6 hours. Besides, BSFC powder was mixed into a solution containing starch powder, which was then stirred to obtain well-dispersed slurries. It was then painted on both sides of the YSZ electrolyte. The resulting disk BSFC||YSZ||BSFC is heated gradually at 500 °C then 1100 °C for 6 hours. The silver paste was used as a current collector on both surfaces of the half-symmetrical cell. AC-impedance analysis Solartron SI 1260 was used to measure the electrical performance at 1 volt and the frequency 0.1 Hz - 32 MHz from room temperature up to 850 °C.

3. Results and discussion

3.1. Structure and microstructure.

The XRD spectra of the calcined powder of electrolyte 8YSZ and electrode BSFC are presented in Figure 1. It shows that 8YSZ has cubic symmetry with lattice parameter a=5.1677 Å having *Fm3m* / 225 symmetry and matched with COD number 2105681 possessing lattice parameter a=5.1546 Å (Ishizawa et al., 1999). On the other hand, the XRD pattern of electrode

material BSFC has cubic symmetry Pm3m / 221 with lattice parameter a=3.9471 Å. Furthermore, a trace peak of the secondary phase at 2θ ≈ 24° was identified as $BaFe_2O_4$.

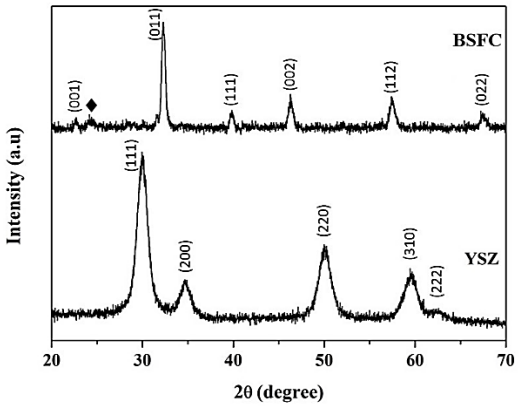

Figure 1. XRD pattern of calcined powder of YSZ and BSFC (♦ = $BaFe_2O_4$).

The crystallite size of the powder should be accomplished through XRD data by the Debye-Scherrer method following the Equation (Muniz et al., 2016):

$$D = \frac{K\lambda}{\beta cos\theta} \quad (1)$$

Where K is the Scherer constant and taken = 0.94 for spherical crystallite with cubic symmetry, λ is the X-ray wavelength = 1.540598 Å, and β is the maximum half-height width (FWHM) of the peak of the XRD spectra. The YSZ's average crystallite size value is ≈11 nm. In the calcined BSFC, the crystalline size was 18 nm, determined by the Debye-Scherrer method. The crystallite size for calcined 8YSZ was clarified by SEM image, as shown in Figure 2. Furthermore, the morphology of crystalline is rounded and agglomerated up to 500 nm.

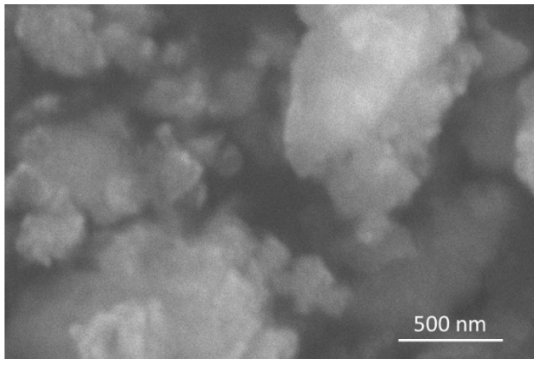

Figure 2. SEM micrograph of YSZ calcined powder.

It is considered that a smaller particle size leads to better densification of the electrolyte powders owing to the higher surface energy of the fine particles. Some factors play a significant role in determining the sintering rate and densification behavior, such as the powder synthesis method, particle size distribution, and post-processing of the powders (Panthi et al., 2018). The sintered electrolyte sample 8YSZ has a relative density of 92 %, while BSFC maintained 61% to facilitate oxygen diffusion. Figure 3a shows the XRD pattern of the sintered YSZ at 1550 ^{0}C for 6h, in which the secondary phase is undetected. It can be considered to have a pure single-phase and homogeneous dissolved dopant distribution. Rietveld's analysis results in a

Cubic structure possessing lattice parameter a = 5.1352 (1) Å and having a figure of merit in the range of the acceptable of refinement: R_{wp}= 11.69, R_p = 9.09, and GoF = 2.45. Figure 3b shows XRD spectra of the electrode after sintering at 1100 ℃ for 6 h. In this case, the secondary phase is identified to have a similar composition but a different structure. The main phase holds cubic perovskite structure Pm3m with lattice parameter a = 3.9469(1) Å, while the secondary phase holds hexagonal symmetry R-3m with lattice parameter a = 5.8499(1) Å and c = 86.4194(1) Å, the reliability factors of the refinement are R_{wp} = 8.38, R_p = 6.70, and GoF = 2.18. The secondary phase quantity was 0.01 mole%. and is supposed to be uninfluencing the electrical properties.

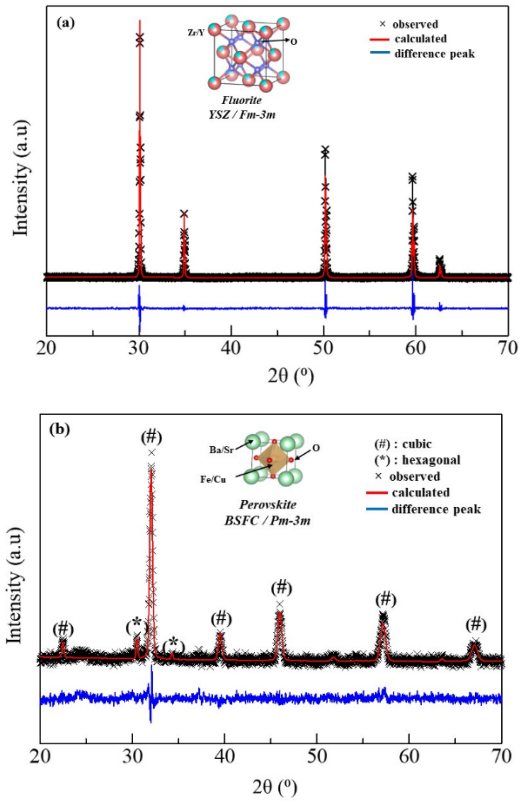

Figure 3. Rietveld's analysis of XRD spectra of sintered sample (a) BSFC and (b) 8YSZ.

3.2. AC-impedance measurement

The half-cell junction of BSFC||YSZ||BSFC is outlined in Figure 4, while the adherent of electrolyte YSZ and electrode BSFC is shown by SEM image. It shows that the two materials are thermally compatible, thereby resulting in good contact between the electrode and the electrolyte.

The impedance complex plot $Z' - Z''$ of the tested samples show differently when temperature increases (Figure 5a-d); however, a similar trend is present in both samples: YSZ and BSFC||YSZ||BSFC. This demonstrates tide coupling between the electrolyte and the electrode, the potential barrier between the two phases is negligible. At low temperatures (below 200 ℃), two semi-circles are shown: at medium temperatures between 250 ℃ - 500 ℃ three semi-circles, while at elevated temperatures 550 ℃ and above, two semi-circles at low frequencies. These semi-circles are related to the resistance of the grains, the grains boundary of YSZ or YSZ+BSFC, and the contact resistance of silver and ceramics BSFC. An electronic circuit model related to the experimental data is proposed in Figure 5a inset. The impedance Z^* response fit with an equivalent circuit model of a serial of two or three loops' circuits of grain R_g - C_g, grain boundary R_{gb} - $C_{gb,}$ and R_{el} – C_{el} depend on the temperature, the dependency of impedance complex Z^*on angular frequency ω then described as follows:

$$Z^* = Z' + jZ'' \tag{2}$$

$$Z' = \frac{R_g}{1+(\omega R_g C_g)^2} + \frac{R_{gb}}{1+(\omega R_{gb} C_{gb})^2} + \frac{R_{el}}{1+(\omega R_{el} C_{el})^2} \tag{2'}$$

$$-Z'' = \frac{\omega R_g^2 C_g}{1+(\omega R_g C_g)^2} + \frac{\omega R_{gb}^2 C_{gb}}{1+(\omega R_{gb} C_{gb})^2} + \frac{\omega R_{el}^2 C_{el}}{1+(\omega R_{el} C_{el})^2} \tag{2''}$$

At low temperatures (Figure 5a), the resistance of the silver electrode is too small compared to the grain and grain boundaries (at the order 10^5 – 10^7 Ω); consequently, it was undetected due to the limitation of low frequency. At the medium temperature (Figure 5b-c), both grain and grain boundary resistance decrease, and the three aspects (grains, grain boundary, and silver contact electrode) become visible. Further elevated temperatures (Figure 5d), the grain resistance becomes too small due to oxygen vacancy $V_O^{\bullet\bullet}$ activate at elevated temperatures to favor conductivity. The small conductivity value needs high frequency to visualize impedance-complex response.

Table 1 shows the numerical values of the resistance and capacitance of grains and grain boundary. The missing data in the table is due to temperature variations, inducing limitations in conserving data. It can be noticed that the grain resistance of YSZ is higher than that of combined BSFC||YSZ||BSFC grains, contrary to grain boundary resistance. It signifies that BSFC grains are more conductive, while grain boundary is more resistive than the YSZ. Furthermore, the grain's capacitance slightly increases with temperature, indicating that the charge carrier population increases on heating.

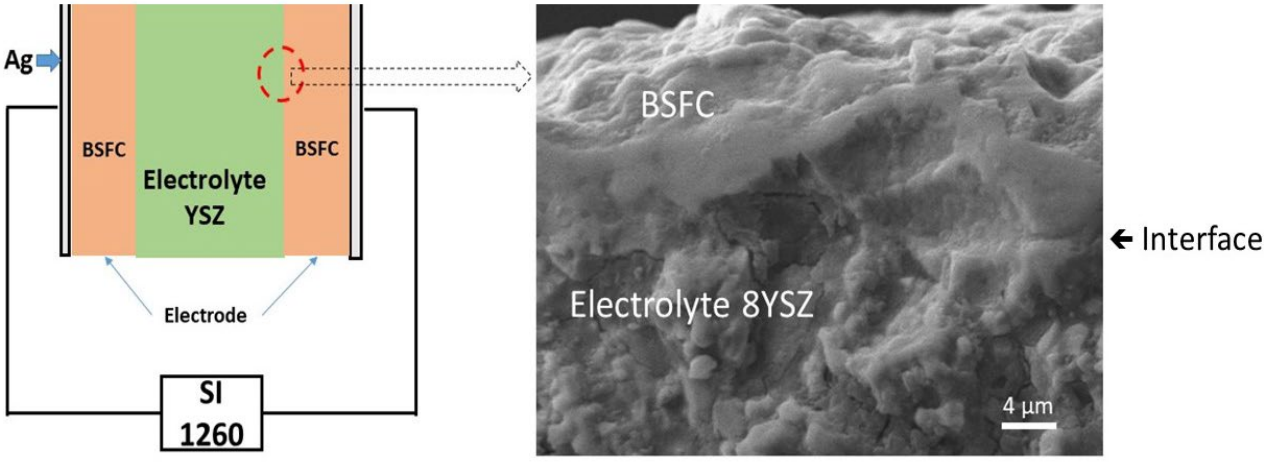

Figure 4. Schematic electrical measurement set-up (left) and cross-section SEM image of the half-cell measurement (right).

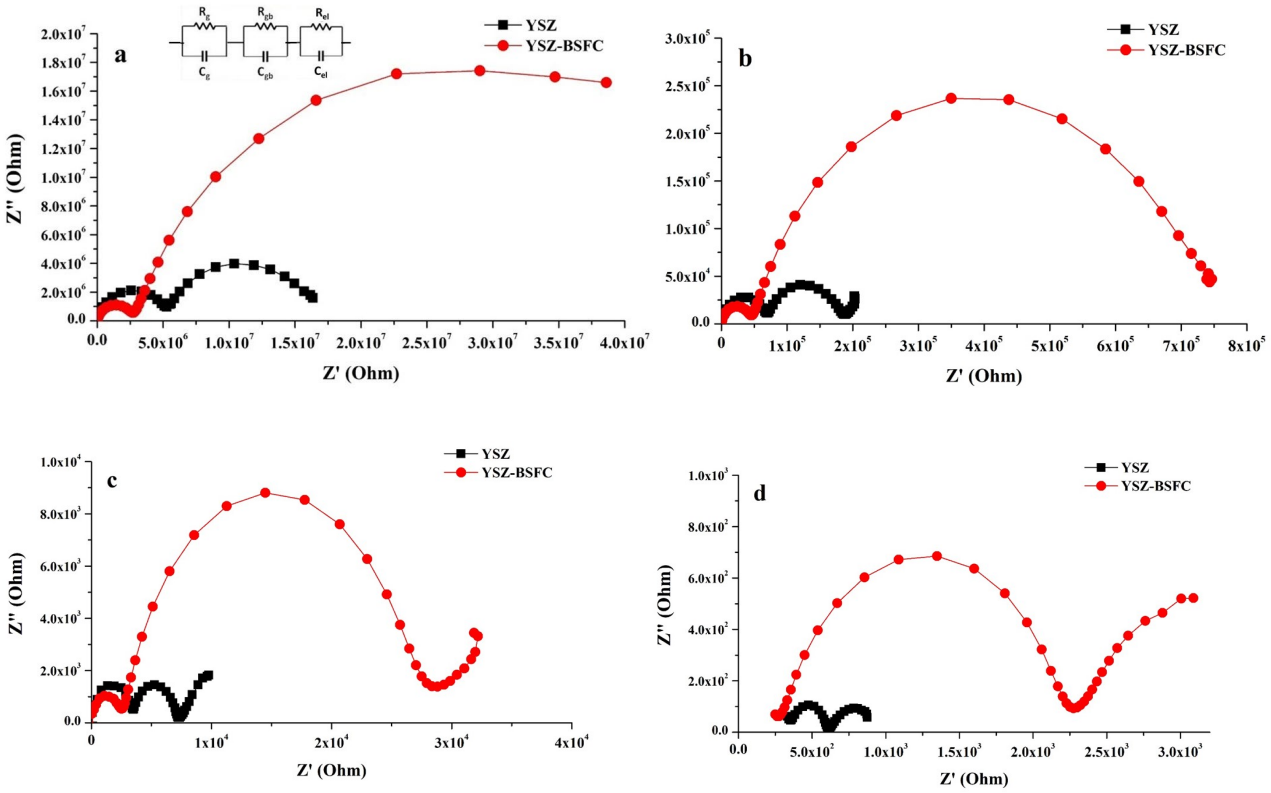

Figure 5. Typical impedance spectra of YSZ polycrystals and half-cell BSFC||YSZ||BSFC measured at different temperatures (a) 200 ^{0}C; (b) 300 ^{0}C; (c) 400 ^{0}C; (d) 500 ^{0}C.

Table 1a. Resistance and capacitance of YSZ at 150 ℃- 500 ℃.

Temperature (^{0}C)	Resistance (Ω)		Capacitance (F)	
	R_{gi}	R_{gb}	C_{gi}	C_{gb}
150	9.60×10^7	1.56×10^8	1.44×10^{-10}	3.98×10^{-9}
200	5.79×10^6	1.37×10^7	1.94×10^{-10}	1.56×10^{-8}
250	3.69×10^5	7.64×10^5	2.66×10^{-10}	4.25×10^{-7}
300	7.65×10^4	1.38×10^5	4.05×10^{-10}	3.91×10^{-7}
350	1.58×10^4	2.11×10^4	4.06×10^{-10}	1.24×10^{-6}
400	3.60×10^3	4.25×10^3	5.92×10^{-10}	3.38×10^{-6}
450	7.84×10^2	1.09×10^3	7.73×10^{-10}	3.65×10^{-6}
500	1.93×10^2	2.88×10^2	1.37×10^{-9}	3.21×10^{-6}
550		1.00×10^2	-	2.08×10^{-6}
600		51.0	-	2.48×10^{-6}
650		34.8	-	2.65×10^{-6}
700		23.6	-	4.50×10^{-6}
750		9.0	-	1.30×10^{-5}
800		9.2	-	1.46×10^{-5}
850		11.2	-	5.55×10^{-5}

Table 1b. Resistance and capacitance of YSZ/BSFC at 150 ℃- 500 ℃.

Temperature (^{0}C)	Resistance (Ω)		Capacitance (F)	
	R_{gi}	R_{gb}	C_{gi}	C_{gb}
150	4.80×10^7	8.20×10^8	1.11×10^{-10}	3.85×10^{-9}
200	3.04×10^6	5.60×10^7	1.43×10^{-10}	7.16×10^{-9}
250	3.14×10^5	4.96×10^6	1.79×10^{-10}	2.64×10^{-8}
300	5.18×10^4	7.78×10^5	2.19×10^{-10}	2.75×10^{-7}
350	1.08×10^4	1.39×10^5	3.38×10^{-10}	2.62×10^{-6}
400	2.90×10^3	2.77×10^4	4.26×10^{-10}	2.16×10^{-6}
450	7.19×10^2	7.21×10^3	5.24×10^{-10}	3.70×10^{-6}
500	1.58×10^2	2.15×10^3	7.93×10^{-10}	3.30×10^{-6}
550		7.30×10^2	-	3.88×10^{-6}
600		2.86×10^2	-	4.38×10^{-6}
650		1.20×10^2	-	4.57×10^{-6}
700		53.6	-	8.99×10^{-6}
750		25	-	3.39×10^{-5}
800		25.8	-	8.36×10^{-5}
850		16.8	-	6.15×10^{-5}

The plot of ln(σT) against 1/T, where σ=1/R is the conductivity of grains and grains boundary of samples, fulfills the Arrhenius character; furthermore, the activation energy values are slightly higher than 1 eV, demonstrating the character of ionic hopping conduction mechanism $V_O^{\bullet\bullet}$ (Omari et al., 2017). The activation energy for the grain and grain boundary conductivity in the temperature range between 150 ^{0}C and 500 ^{0}C are listed in Figure 6 inset. This deduction matched with Zhang et al. (2020) for electrolyte Y-doped Zirconia (Figure 6) (Zhang et al., 2020). For both samples, the grain conductivity is higher than the grain boundary conductivity at all measured temperatures.

The dependencies of real impedance *Z'* and imaginary impedance *Z''* on angular frequency are presented in Figure 7a-b. The impedance *Z'* shows steps related to the resistance of the circuit, high frequency related to R_g, medium frequency related to R_g+R_{gb}, and low frequency related to R_g+R_{gb}+R_{el}. The transition between the two steps indicates Debye's relaxation, which is clearly shown by *Z''*, Figure 7b, the relaxation frequency $\omega_{max(i)} = 1/R_iC_i$. At low frequencies, it is related to the space charge response long-range movement, and the high impedance results from the grain boundary potential barrier, which deteriorates when the temperature upsurges. At high frequencies, the response is linked to the short movement of the charge carrier in the grain response, while at the medium frequency, it is associated with the grain boundary. It shows that $\omega_{max(i)}$ shifts to high frequency through temperature, suggesting an increase of charge carrier of oxygen vacancy at elevated temperature.

Further analysis of the electrode parameters was conducted at an elevated temperature, *vis a vis* the operating intermediate temperature of solid oxide fuel cell (IT-SOFC) as shown in Figure 8. Taking the Debye relaxation frequency and radius, the numerical values of electrodes measure R and C then determined and presented in Table 2. It shows numerical values of R and C are greater on BSFC||YSZ||BSFC connected system compared with YSZ only. This demonstrates the connecting system generates barrier potential. Otherwise, contact resistance, as well as the trapped charges, induce capacitance formation.

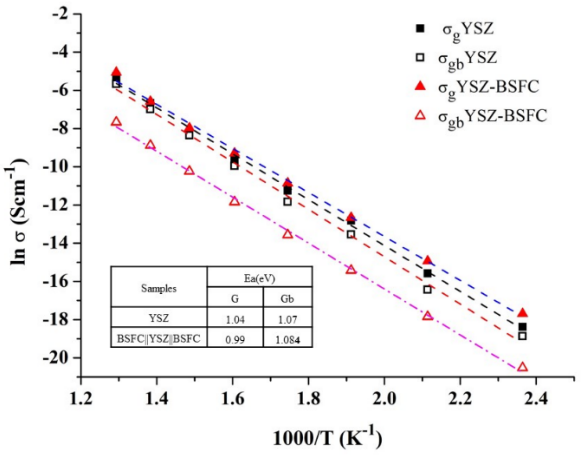

Figure 6. Arrhenius plot of grain and grain boundary conductivity of YSZ and BSFC||YSZ||BSFC at 150 - 500^{0}C.

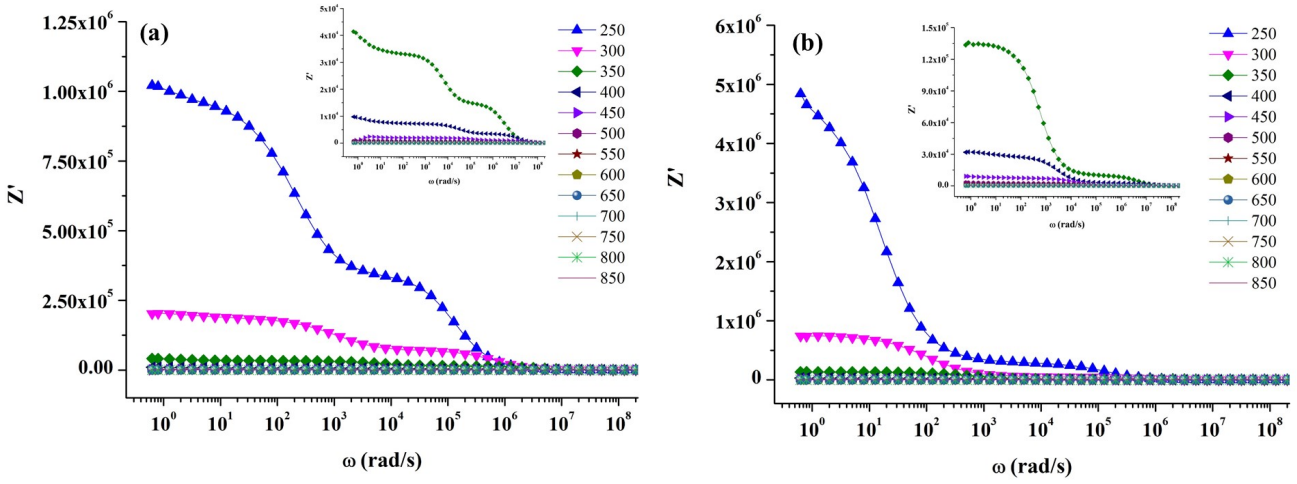

Figure 7. Variation of the real part of the impedance as a function of the frequency at various temperatures of (a) YSZ and (b) YSZ/BSFC.

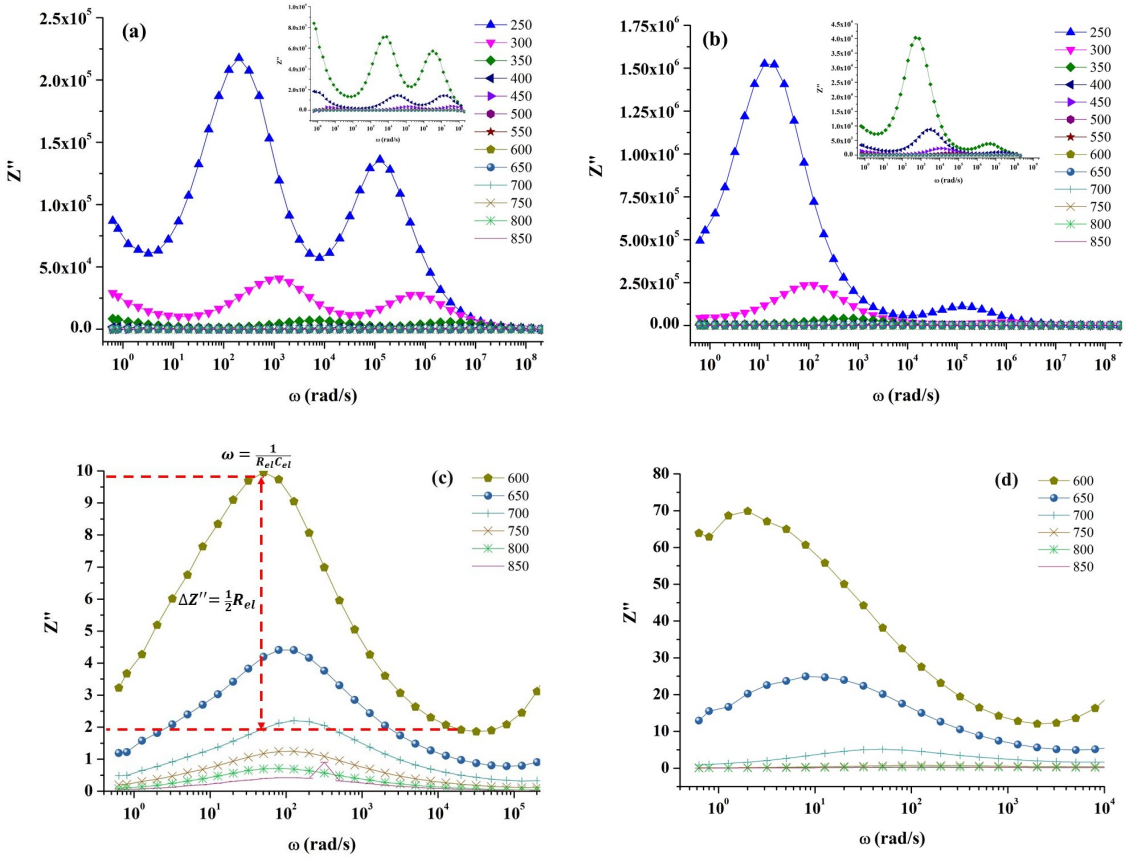

Figure 8. Variation of the imaginary part of the impedance as a function of frequency and temperature of (a) YSZ, (b) BSFC||YSZ||BSFC, elevated temperature and low-frequency parts of (c) YSZ and (d) BSFC||YSZ||BSFC.

Table 2. Data summary of AC impedance measurement.

Sample	Temperature (°C)	ω(rad.s^{-1})	$R_{electrode}$ (Ω)	$C_{electrode}$
YSZ	600	50.4788	19.9097	0.0009
	650	80.0036	8.8177	0.0014
	700	126.7972	4.4104	0.0017
	750	126.7972	2.4946	0.0031
	800	126.7972	1.3858	0.0056
	850	126.7972	0.8442	0.0093
YSZ/BSFC	600	2.0096	139.7318	0.0035
	650	12.6797	49.4041	0.0015
	700	50.4788	10.2467	0.0019
	750	126.7972	1.5281	0.0051
	800	126.7972	0.7145	0.0110
	850	200.9600	0.4842	0.0102

4. Conclusion

In this study, 8YSZ and BSFC were successfully synthesized via the sol-gel self-combustion method, and their electrical conductivity was characterized. YSZ powder was calcined at 700℃ for 2 hours, then pressed into a disk and sintered at 1550 ^{0}C for 6 hours. While BSFC powder calcined at 850 ℃ for 6 hours and sintered at 1100 ^{0}C for 6 hours. The structure was analyzed using XRD; 8YSZ has a cubic structure with space group Fm-3m, while BSFC also has a cubic structure with space group Pm-3m. The lattice parameter of the 8YSZ was calculated using the Rietveld method and obtained 5.17 Å, and the crystalline size of 8YSZ was analyzed using the Debye-Scherrer equation and analyzed using MAUD software and got 10.90 ± 1.54 nm and 10.93 ± 0.12 nm, respectively. Scanning electron microscope (SEM) shows that BSFC can adhere well to the surface of YSZ to build half-cell configuration BSFC||YSZ||BSFC. The electrical behavior of both samples measured at 150℃ - 850 ^{0}C shows three responses. At low temperatures (below 200 ℃), two semi-circles, between 250 ℃ - 500 ℃ three semi-circles, while at 550 ℃ and above, two semi-circles. These semi-circles are related to the resistance of the grains, the grains boundary of YSZ or YSZ+BSFC, and the electrode. The Z' - Z'' plot analysis and spectra of Z' and Z'' against frequency revealed that the resistivity decreased with increasing temperature. Furthermore, the overall resistivity of BSFC||YSZ||BSFC system is lower than YSZ due to the influence of BSFC. However, Debye's relaxation at low frequency and high-temperature analysis shows the connected system generates barrier potential, finally, cathode material BSFC is suitable for YSZ electrolyte.

Conflict of interest

The authors have no conflict of interest to declare.

Funding

The authors received no specific funding for this work.

References

Budiana, B., Fitriana, F., Ayu, N., & Suasmoro, S. (2016). Preparation and conductivity measurement of 7-8 mol% YSZ and 12 mol% CSZ for electrolyte SOFC. In *Journal of Physics: Conference Series* (Vol. 739, No. 1, p. 012022). IOP Publishing. https://doi.org/10.1088/1742-6596/739/1/012022

Dong, Y., & Chen, I. W. (2018). Oxygen potential transition in mixed conducting oxide electrolyte. *Acta Materialia*, *156*, 399-410. https://doi.org/10.1016/j.actamat.2018.06.014

Fitriana, F., Baity, P. S. N., Zainuri, M., Kidkhunthod, P., & Suasmoro, S. (2021). Crystal structure and Cu/Fe K-edge analysis of $Ba_{0.5}Sr_{0.5}Fe_{1-x}Cu_xO_{3-\delta}$ (x=0–0.2)and the influence on conductivity. *Journal of Physics and Chemistry of Solids*, *154*, 110065. https://doi.org/10.1016/j.jpcs.2021.110065

Fitriana, F., Anjarwati, D. Z., Baity, P. S. N., & Suasmoro, S. (2018). Synthesis of Nanocrystalline Ba $_{0,5}Sr_{0,5}FeO_{3-\delta}$ by Sol-gel Self-Combustion Method. In *IOP Conference Series: Materials Science and Engineering* (Vol. 395, No. 1, p. 012011). IOP Publishing.
https://doi.org/10.1088/1757-899X/395/1/012011

Hunter, B. A. (2000). Rietica-A visual Rietveld program.
https://inis.iaea.org/search/search.aspx?orig_q=RN:31059005

Peláez-Tirado, I. M., Marín-Rueda, J. R., Ramos-Fajardo, J. M., Jiménez, J. F. V., Castro-García, M., Pérez-Flores, J. C., & Canales-Vázquez, J. (2024). Fused filament fabrication and characterisation of 3-and 8-YSZ-based SOFC electrolytes. *Journal of the European Ceramic Society*, *44*(8), 5031-5040.
https://doi.org/10.1016/j.jeurceramsoc.2024.02.007

Ishizawa, N, Matsushima, Y, Hayashi, M & Ueki, M. (1999). Synchrotron radiation study of yttria-stabilized zirconia $Zr_{0.758}Y_{0.242}O_{1.879}$. *Acta Crystallographica Section B: Structural Science, 55* (5), 726-735.
https://doi.org/10.1107/s0108768199005108

Muniz, F. T. L., Miranda, M. R., Morilla dos Santos, C., & Sasaki, J. M. (2016). The Scherrer equation and the dynamical theory of X-ray diffraction. *Acta Crystallographica Section A: Foundations and Advances*, *72*(3), 385-390.
https://doi.org/10.1107/S205327331600365X

Omari, L. H., Moubah, R., & Haddad, M. (2017). Conductivity and electrical impedance of $(BaTiO_3)_{0.95}$ -$(LaFeO_3)_{0.05}$ solid solutions. *Materials Chemistry and Physics*, *199*, 138-143.
https://doi.org/10.1016/j.matchemphys.2017.06.046

Panthi, D., Hedayat, N., & Du, Y. (2018). Densification behavior of yttria-stabilized zirconia powders for solid oxide fuel cell electrolytes. *Journal of Advanced Ceramics*, *7*, 325-335.
https://doi.org/10.1007/s40145-018-0282-4

Sato, K., Horiguchi, K., Nishikawa, T., Yagishita, S., Kuruma, K., Murakami, T., & Abe, H. (2015). Hydrothermal synthesis of yttria-stabilized zirconia nanocrystals with controlled yttria content. *Inorganic Chemistry*, *54*(16), 7976-7984.
https://doi.org/10.1021/acs.inorgchem.5b01112

Schäfer, J., Sigmund, W., Roy, S., & Aldinger, F. (1997). Low temperature synthesis of ultrafine Pb (Zr, Ti) O3 powder by sol-gel combustion. *Journal of Materials Research*, *12*(10), 2518-2521.
https://doi.org/10.1557/JMR.1997.0333

Wang, Q., Peng, R., Xia, C., Zhu, W., & Wang, H. (2008). Characteristics of YSZ synthesized with a glycine-nitrate process. *Ceramics International*, *34*(7), 1773-1778.
https://doi.org/10.1016/j.ceramint.2007.06.003

Wang, J., Saccoccio, M., Chen, D., Gao, Y., Chen, C., & Ciucci, F. (2015a). The effect of A-site and B-site substitution on $BaFeO_{3-\delta}$: An investigation as a cathode material for intermediate-temperature solid oxide fuel cells. *Journal of power sources*, *297*, 511-518.
https://doi.org/10.1016/j.jpowsour.2015.08.016

Wang, J., Lam, K. Y., Saccoccio, M., Gao, Y., Chen, D., & Ciucci, F. (2015b). Ca and In co-doped $BaFeO_{3-\delta}$ as a cobalt-free cathode material for intermediate-temperature solid oxide fuel cells. *Journal of Power Sources*, *324*, 224-232.
https://doi.org/10.1016/j.jpowsour.2016.05.089

Zakaria, Z., Abu Hassan, S. H., Shaari, N., Yahaya, A. Z., & Boon Kar, Y. (2020). A review on recent status and challenges of yttria stabilized zirconia modification to lowering the temperature of solid oxide fuel cells operation. *International Journal of Energy Research*, *44*(2), 631-650.
https://doi.org/10.1002/er.4944

Zarkov, A., Stanulis, A., Sakaliuniene, J., Butkute, S., Abakeviciene, B., Salkus, T., ... & Kareiva, A. (2015). On the synthesis of yttria-stabilized zirconia: a comparative study. *Journal of Sol-Gel Science and Technology*, *76*, 309-319.
https://doi.org/10.1007/s10971-015-3778-1

Zhang, J., Lenser, C., Menzler, N. H., & Guillon, O. (2020). Comparison of solid oxide fuel cell (SOFC) electrolyte materials for operation at 500 °C. *Solid State Ionics*, *344*, 115138.
https://doi.org/10.1016/j.ssi.2019.115138